Onion skin model (OSM) analysis of EAST SOL plasmas

2014 Nucl. Fusion 54 093002

(http://iopscience.iop.org/0029-5515/54/9/093002)

IOP Publishing | International Atomic Energy Agency Nuclear Fusion
Nucl. Fusion **54** (2014) 093002 (11pp) doi:10.1088/0029-5515/54/9/093002

Onion skin model (OSM) analysis of EAST SOL plasmas

F.Q. Wang[1], Y.P. Chen[1], L.Q. Hu[1], H.Y. Guo[1,2,3], S.C. Liu[1] and L. Wang[1]

[1] Institute of Plasma Physics, Chinese Academy of Sciences, Hefei 230031, Anhui, People's Republic of China
[2] School of Nuclear Science and Technology, University of Science and Technology of China, Hefei 230027, Anhui, People's Republic of China
[3] General Atomics, PO Box 85608, San Diego, CA 92186, USA

E-mail: wangfq@ipp.ac.cn

Received 13 January 2014, revised 19 May 2014
Accepted for publication 24 June 2014
Published 30 July 2014

Abstract

Two-dimensional maps of the Experimental Advanced Superconducting Tokamak (EAST) scrape-off layer (SOL) plasma conditions for ohmic, L-mode and H-mode discharges are reconstructed using an onion skin model (OSM) coupled in DIVIMP together with the Monte Carlo neutral transport code, EIRENE. The boundary conditions for OSM calculation are taken from the measurements of the Langmuir probe built into the divertor targets. The OSM-calculated values of the outboard mid-plane electron density, n_e, and temperature, T_e, are compared with the mid-plane measurements of n_e and T_e from a fast reciprocating probe. Some other characteristics of these SOL plasmas are also derived from the OSM solution, reflecting that the upstream plasma conditions are governed by the SOL collisionality to a large degree. Values of $\chi_\perp^{SOL}$ at the low-field side and the high-field side mid-plane are derived separately as a function of the distance to the separatrix for ohmic, L- and H-mode discharges, showing that $\chi_\perp^{SOL}$ increases with the distance to the separatrix at both sides and that the values of $\chi_\perp^{SOL}$ at the low-field side tends to be higher than that at the high-field side. $\chi_{\perp e}^{SOL}$ is found to be larger than $\chi_{\perp i}^{SOL}$ by a factor of 2–3 for all the discharges considered here. In addition, before the use of the OSM method of extracting $\chi_\perp^{SOL}$ and $D_\perp^{SOL}$ for EAST discharges, the reliability of this method is assessed by taking SOLPS-generated target n, T profiles as boundary conditions and by comparing the OSM-extracted cross-field transport coefficients with those input in the SOLPS modelling.

Keywords: onion skin model (OSM), SOL, EAST, cross-field transport

(Some figures may appear in colour only in the online journal)

1. Introduction

The scrape-off layer (SOL) [1], the region of open magnetic field lines outside the separatrix established by a diverting magnetic field, provides interfaces between the plasma and the ordinary solid-state surfaces. The heating and erosion of the plasma-facing components (PFCs) are mainly governed by particle and heat flows reaching the solid surface, especially by their relation to the density and temperature distribution in the SOL. The transport properties of impurities released from PFCs due to the impact of plasma ions, however, are likely to be governed by the detailed information about the electrostatic field $\boldsymbol{E}$ and the plasma flow field $\boldsymbol{V}$, as well as by thermal and frictional forces exerted by gradients in the SOL temperature and pressure profiles. Thus, knowing the spatial distribution of SOL plasma conditions (n_e, T_e, T_i, $\boldsymbol{E}$, $\boldsymbol{V}$) is very fundamental to carry out a detailed analysis of the physics processes occurring there.

The cross-field particle diffusivity ($D_\perp^{SOL}$) and thermal heat diffusivity ($\chi_\perp^{SOL}$) are considered to be key parameters determining the SOL physics processes in a tokamak [2, 4]. These parameters cannot be derived from first principles, but are all anomalous. To determine them, the radial profiles of density and temperature are needed at two or more places along the SOL. Due to the fact that two-dimensional (2D) edge fields (n_e, T_e, T_i, $\boldsymbol{E}$, $\boldsymbol{V}$) are not fully measured on tokamaks, modelling work is inevitably involved in the SOL behaviour analysis activities, including identification of cross-field transport coefficients, etc.

One approach to establishing a 2D map of SOL plasma conditions is using, for example, the SOLPS code [3] to solve 2D conservation equations with upstream boundary conditions, typically the density on a closed flux surface near the separatrix and the power outflow from the main plasma to the boundary. In SOLPS, the anomalous transport coefficients $\chi_\perp^{SOL}$ and $D_\perp^{SOL}$ are given as input and, for example, can be

assumed to be spatially constant and can be adjusted to try to match the measured n, T profiles at some location, e.g. divertor targets, in the SOL. In the case of SOLPS, the B2 code is coupled to the 3D Monte Carlo neutral transport code, EIRENE [5, 6] in order to model the neutral behaviours.

An alternative SOL modelling approach is using the so-called 'onion skin' model (OSM) [1], in which the SOL is divided into several, along-$\boldsymbol{B}$, flux tubes nested inside each other and 1D, along-$\boldsymbol{B}$, modelling is carried out for each flux tube separately, treating the cross-field terms more or less simply. The boundary conditions (n_e or J_{sat}, T_e, T_i) of each flux tube are specified across the divertor targets, ideally from the experimental measurements, for example using Langmuir probes. The interaction of the plasma with the recycled hydrogen neutrals and the associated source/sink terms are considered by coupling to EIRENE. The 2D plasma solution is achieved by analysing the parallel and cross-field balances (i.e. particle/power balance) sequentially and iteratively. Unlike the SOLPS modelling, the values of $\chi_\perp^{SOL}$ and $D_\perp^{SOL}$ do not need to be input in the OSM-based modelling, but can be extracted from the generated 2D plasma conditions [26].

The OSM-based interpretive modelling has several advantages [1, 7] over the SOLPS modelling. For example, a larger amount of experimental information can be used as input, and the cross-field transport is implicitly included in the boundary conditions (target n, T profiles) of OSM analysis [1, 12]. Also, convergent solutions are more rapidly obtained in OSM analysis since the plasma conditions at the divertor targets are fixed [7] and the fluid equations to be solved by the OSM are just 1D. However, the more or less simplified assumptions [1] used in the OSM analysis must be validated, usually, by comparing the results against the experimental measurements.

For these reasons, the OSM is widely used to analyse the edge measurements for tokamaks, such as JET [7–11], DIII-D [12], MAST [11, 13], etc. OSM-based SOL plasma analysis carried out on these tokamaks has obtained lots of useful information on the SOL physics processes, especially the information about the SOL cross-field heat and particle transport property ($\chi_\perp^{SOL}$, $D_\perp^{SOL}$) of these tokamaks. Since the target power deposition width λ_q, one of the most critical quantities in the development of magnetic fusion energy, is largely affected by the SOL cross-field heat transport, a study on the SOL plasmas, especially the SOL cross-field heat transport properties in the present tokamak experiment devices, can give hints on how to control and scale λ_q to future devices. Carrying out the parallel OSM method of SOL study on the Experimental Advanced Superconducting Tokamak (EAST) device is of great importance.

In this paper, results from OSM modelling for a series of single-null (SN) divertor ohmic, L- and H-mode discharges on EAST are presented and the cross-field transport coefficients are also extracted. Section 2 briefly introduces the edge physics process related experimental measurement on EAST. Section 3 discusses the model being used and data being modelled. Section 4 provides a comparison of upstream parameters generated by the OSM with measurements from a fast reciprocating probe (FRP), as well as some other characteristics of EAST SOL plasmas derived from the OSM. Section 5 gives a full comparison between the OSM-generated 2D SOL plasma conditions and the SOLPS-calculated ones followed by the extraction of cross-field heat diffusivity in the SOL together with some preliminary observations on the characteristics of SOL heat transport in EAST. The summary and conclusions are given in section 6.

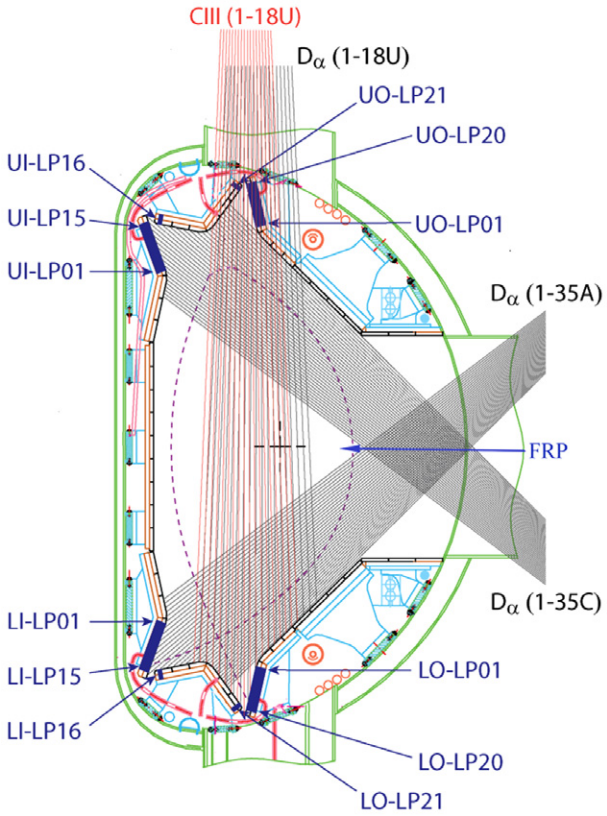

Figure 1. Edge process related diagnostics on the EAST device.

2. Edge process related diagnostics on EAST

EAST, the first fully superconducting tokamak in the world, is designed to study key issues of plasma physics and fusion technology in steady-state operation in support of ITER [14]. This device has been developed with the design parameters shown in [15]. It can operate with limiter and various poloidal divertor configurations, including the lower single null (LSN), upper single null (USN) and double null (DN) configurations. On EAST device, the first operation was started in 2006, and sequential experimental campaigns have been implemented with gradually upgraded engineering conditions and physics goals since then. During the 2010 experimental campaign, discharges with stationary ELMy H-mode confinement were successfully achieved in EAST with both LSN and DN divertor configurations.

To facilitate the scientific research carried out on the EAST device, various diagnostics with respect to edge plasma behaviours have been carried out and gradually upgraded. These measurements provide lots of useful information for the analysis of EAST SOL physics processes [15–17]. The poloidal cross-sectional disposition of edge process related diagnostics on the EAST device is shown in figure 1, including built-in Langmuir probe arrays across the four divertor targets

(lower inner (LI-LP01–LI-LP16), lower outer (LO-LP01–LO-LP21), upper inner (UI-LP01–UI-LP16), upper outer (UO-LP01–UO-LP21)), a FRP at the outer mid-plane, the D_α signal viewing chords (D_α (1-35A), D_α (1-35C), D_α (1-18U)) covering both the lower and the upper divertor regions, and the C III spectral signal viewing chords (C III (1-18U)). Each of them can shed light on one or more physics processes occurring in the edge. However, the measurements can be combined together with the results from the OSM coupled with the Monte Carlo neutral transport code, EIRENE, and DIVIMP impurity transport code to allow at least some understanding of the overall SOL plasma transport [18, 19, 23].

Although these various diagnostics introduced above have been implemented on the EAST device, due to the fact that this device is still at its preliminary operation stage, some other useful diagnostics such as a lithium beam for the measurement of upstream density and the edge Thomson scattering diagnostic system have not yet been implemented on EAST (Thomson scattering diagnostics system on EAST just mainly covers the main plasma region). At present, target probe data are available for more discharges than upstream probe data on the EAST device. That is because the upstream probes are not able to penetrate into the separatrix in high-power, high-density discharges for the risk of damage. These problems in the present EAST edge process related diagnostics make OSM analysis for EAST SOL plasmas slightly difficult, but this does not mean that there is no possibility or no need to use this method to do some useful work for EAST.

In common with all the other tokamaks, uncertainties in the reconstruction of the magnetic configuration, e.g. using EFIT, i.e. uncertainties in the separatrix location at both the target location and the mid-plane location are inevitable on EAST. For this reason, some shifting is needed for any comparison of target and upstream profiles on EAST. According to [8, 11], the separatrix at the target location is sometimes identified by assuming that one of the target profiles, say the J_{sat} profile, peaks at the true separatrix. This then allows an approach in which one works from the target data using the OSM to calculate the upstream conditions and compares the OSM-calculated upstream n, T profiles with the shifted FRP profiles. For the code–experiment comparison presented in this paper, the FRP profiles are shifted so that the OSM and FRP T_e values match at the separatrix location. It is remarkable that due to the losses of particles, momentum and energy into the private flux zone, PFZ, which 'erode' the target profiles, the peak of the J_{sat} profile, generally, occurs some distance away from the true separatrix [27]. That is, generally, the assumption that the J_{sat} profile peaks at the true separatrix is not correct. However, all the conclusions presented in this paper will be little affected by this assumption.

One thing to be noted is that the target Langmuir probes only directly measure T_e and J_{sat}, thus sometimes n_e must be derived, usually by assuming $T_e = T_i$, from $J_{sat} \approx 0.5 n_e c_s$, where $c_s \approx [k(T_e + T_i)/m_i]^{1/2}$ is the ion-sound speed. This temperature equilibration assumption seems to be reasonable and more likely to hold at the target, due to the stronger collisionality there. While for the less collisional upstream conditions, $T_{iu} > T_{eu}$ is anticipated [21, 22].

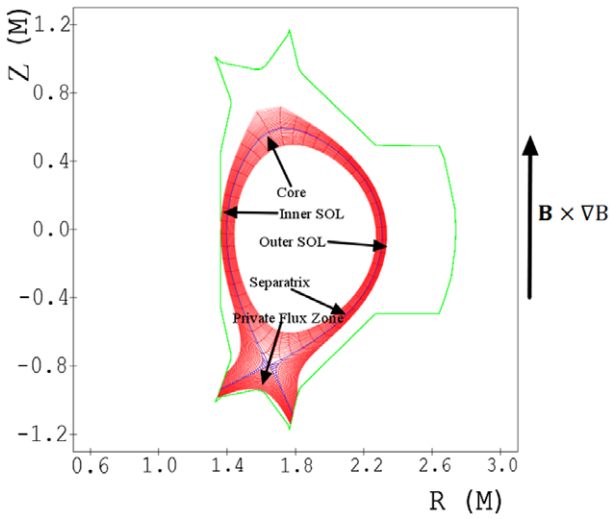

Figure 2. Grid used for the OSM analysis.

3. The interpretive 'onion skin' model and the data to be modelled

3.1. Data to be modelled

'Onion skin' modelling in combination with the Monte Carlo code, EIRENE and DIVIMP, for edge analysis has previously only been developed for interpretive analysis of SN divertor plasmas. Although EAST can operate with both SN and DN divertor configurations, this paper will only focus on OSM analysis of EAST SOL plasmas with SN divertor configurations, including both the USN and the LSN divertor configurations. Figure 2 shows a 2D grid generated from the magnetic reconstruction for a typical EAST LSN divertor configuration. This quasi-orthogonal grid (non-orthogonal near the divertor targets) shown in figure 2 can be used by both the SOLPS modelling and the OSM–EIRENE–DIVIMP modelling, which facilitates the direct comparison between the SOLPS-generated plasma conditions and the OSM-generated ones. The definition of the calculation regions for the OSM-based analysis and the direction of the ion $\mathbf{B}\times\nabla B$ drift are also shown in this figure. Note that on EAST, the ion $\mathbf{B}\times\nabla B$ drift is directed towards the upper divertor, which is just the opposite of that on other tokamaks, such as JET and MAST. The grid for OSM analysis consists of 'poloidal rings' aligned to the flux surfaces, extending from one target to the other along the SOL in the poloidal plane. With the knowledge of the local values of the magnetic pitch angle from magnetic pick-up signals, one can work with one coordinate parallel to $\boldsymbol{B}$ and the other coordinate in the cross-field (radial) direction.

Several shots in attached regimes (attached at both the inner target and the outer target) are chosen, including ohmic and L-mode discharges with both LSN and USN divertor configurations and one H-mode discharge with LSN divertor configuration. The main characteristics of the discharges modelled are given in table 1. All these shots are deliberately chosen to have good target profiles. Unfortunately, due to the fact that upstream probes are not able to penetrate into the separatrix in high-power, high-density discharges for the risk of damage, this H-mode discharge has no FRP data.

Table 1. Main characteristics of the discharges modelled in this study; LHW, low hybrid wave; ICRH, ion cyclotron resonant heating.

Shot no	Time (s)	Type	I_p (MA)	$\bar{n}_e(10^{19}\ m^{-3})$	B_T (T)	P_{in} (MW)	q_{95}	a(m)	R(m)	Config.
41594	5.25	Ohmic	0.398	1.614	1.806	0.285 (ohmic)	4.166	0.432	1.861	LSN
41594	7.10	Ohmic	0.399	1.5361	1.806	0.266(ohmic)	3.975	0.442	1.860	USN
31737	7.40	L	0.403	0.98	1.806	0.150(ohmic) +0.200(LHW)	5.020	0.448	1.855	LSN
31737	4.20	L	0.401	0.82	2.011	0.134(ohmic) +0.167(LHW)	4.356	0.446	1.860	USN
41825	3.90	H	0.502	4.85	1.806	0.38(ohmic) +1.2(LHW) +0.3(ICRH)	3.674	0.437	1.880	LSN

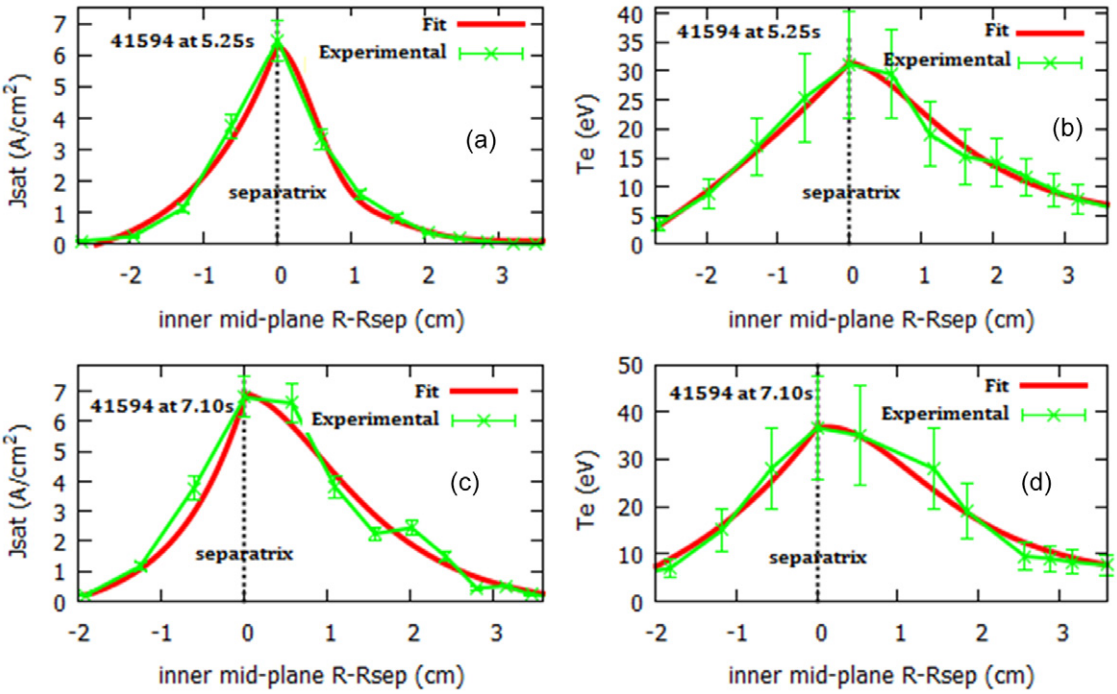

Figure 3. Measured lower inner divertor target profiles of T_e and J_{sat} for shot 41594 at 5.25 s and the upper inner divertor target T_e and J_{sat} profiles for shot 41594 at 7.10 s.

Using the data from the target Langmuir probes, the position of the strike points and the flux expansion between the mid-plane and the targets, the measured target T_e and J_{sat} are mapped to the mid-plane and plotted as a function of distance to the separatrix. In order to interpolate the experimental data onto the grid, one has to fit the data in a particular form. According to [11], exponential profiles with the form $\alpha e^{(x_o-x)/\lambda_{1,2}}$ are fitted to the EAST target data and then mapped back onto the target resulting in Gaussian profiles in the SOL while still exponential profiles in the PFZ [24]. Here x_0 corresponds to the peaks of the distribution and λ_1 is the $1/e$ decay length for the private flux region and λ_2 is the $1/e$ decay length for the SOL region. The grid data are mapped onto these fitted target profiles and the target T_e and J_{sat} parameters are determined for each grid cell at the target. Figures 3 and 4 illustrate the T_e and J_{sat} target profiles for shot 41594 at 5.25 and 7.10 s. In these two figures, the green coloured points represent the experimental data, and the red coloured lines represent the fitting to the measured profiles.

3.2. The onion skin model (OSM)

Here, in this paper, a sophisticated OSM solver based on Runge–Kutta numeric computation is chosen to use. The conservation equations [1] used in this OSM solver can be illustrated in detail as follows:

$$\frac{d}{ds}\left[\frac{5}{2}.n(s).v\,(s)\,.kT_e(s) - \kappa_{0e}.T_e\,(s)^{\frac{5}{2}}\frac{dT_e\,(s)}{ds}\right] = -P_{rad} - P_{helpi} - P_{ei} \quad (1)$$

$$\frac{d}{ds}\left[\frac{5}{2}.n(s).v\,(s)\,.kT_i(s) - \kappa_{0i}.T_i\,(s)^{\frac{5}{2}}\frac{dT_i\,(s)}{ds} + \frac{1}{2}n(s)mv(s)^3\right] = -P_{cx} + P_{ei} \quad (2)$$

$$\Gamma(s)=n(s)v\,(s)=n_0v_0 + \int_0^s S\left(s'\right)ds' \quad (3)$$

$$n(s)\left[(kT_e\,(s) + kT_i(s)) + mv\,(s)^2\right] = \left(1 + M_t^2\right)(kT_{e0} + kT_{i0}) \quad (4)$$

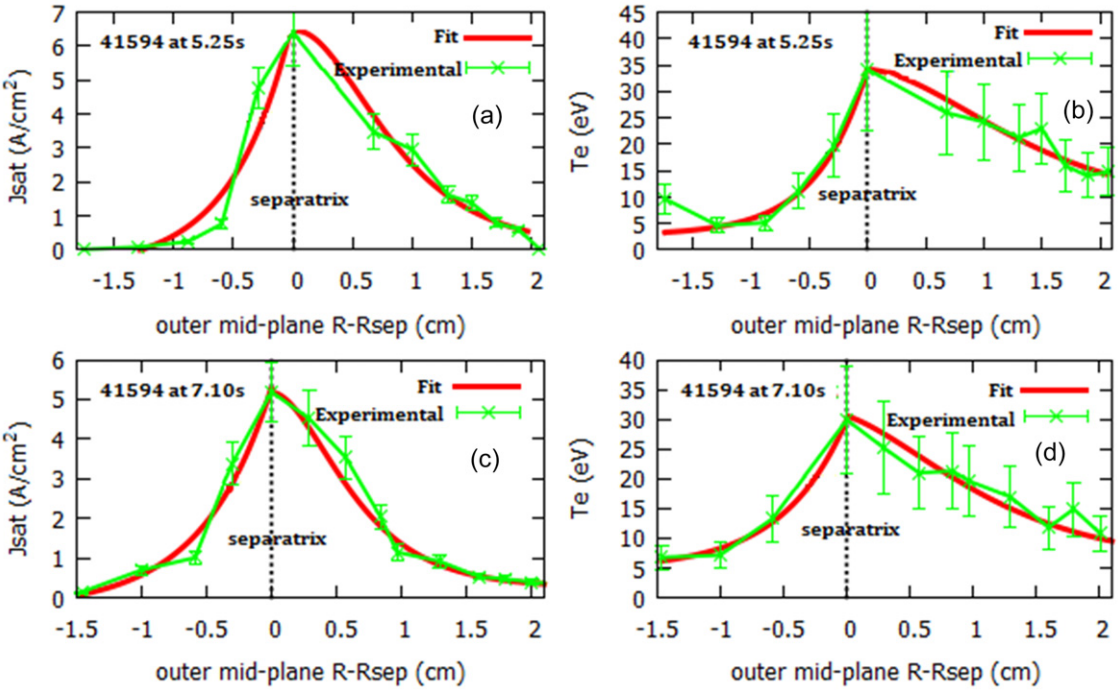

Figure 4. Measured lower outer divertor target profiles of T_e and J_{sat} for shot 41594 at 5.25 s and the upper outer divertor target T_e and J_{sat} profile for shot 41594 at 7.10 s.

where s, in these equations, is the distance along-$\boldsymbol{B}$ from the target, $T_e(s)$, $T_i(s)$, $n(s)$, $v(s)$ are the along-$\boldsymbol{B}$ background plasma parameters, the electron temperature, ion temperature, density and the plasma flow velocity, respectively. Equations (1) and (2) are the illustration of electron and ion power conservation, respectively. The terms, $\frac{5}{2}n(s)v(s)kT_{e,i}(s)$ and $\kappa_{0e,i}.T_{e,i}(s)^{\frac{5}{2}}\frac{dT_{e,i}(s)}{ds}$, in equations (1) and (2) are the contribution of electron/ion parallel heat convection and conduction to the electron/ion power conservation, where κ_{0e} and κ_{0i} are the electron and ion conduction constant, with typical values $\kappa_{0e} = 2000$, $\kappa_{0i} = 59$. Convection and some other important terms, such as P_{helpi}, the cooling of electron caused by inelastic collision associated with recycling of hydrogen neutrals, and P_{cx}, charge exchange heating/cooling of ions, as well as ionization rate, $S(s)$ in the particle conservation equation (3), are obtained by coupling OSM to the Monte Carlo neutral transport code, EIRENE. Ideally, detailed information about the strength and spatial distribution of P_{rad}, radiation loss of the impurities and the background plasma, given by the DIVIMP code would be automatically fed back to the OSM solver and these two codes should be run iteratively to convergence. However, this true feedback mode is still under development. In the OSM modelling presented here, the total strength and spatial distribution of P_{rad} are specified and adjusted by hand under the guidance of DIVIMP outputs. As with studies presented in [7–13], this paper will only focus on the background plasmas, and a detailed report on DIVIMP impurity analysis will be given later. The term, $\frac{1}{2}n(s)mv(s)^3$, in equation (2) is the kinetic convection term for ions. Equation (4) is the description of momentum conservation, which clearly shows that friction and viscosity are not taken into consideration in the modelling. In the modelling work presented here, the target Mach number M_t is set to 1, which means that, v_0, the plasma flow velocity at the divertor target is assumed to be the target iono-acoustic velocity. T_{e0}, T_{i0}, n_0 are divertor target plasma conditions, usually taken from the built-in Langmuir probe measurements. All these terms appearing in the above equations can be turned on/off or adjusted by options/switches in the input file.

Simplified assumptions about the cross-field flows are inevitable in the OSM analysis. For a particular flux tube, the power flow to the target, $q_{\parallel t}$, and any volumetric power sinks in that tube must be supplied by the cross-field power flow. Where did the cross-field power flow enter that tube? Actually, the cross-field heat source is distributed spatially in a very complex way. However, it has been proven in [8, 25] that the upstream plasma solution is quite insensitive to the assumption about the spatial distribution of the cross-field power sources. Here, in this paper, the cross-field power sources are assumed to distribute uniformly along the flux tube. In the modelling presented here, $q_{\parallel t}$ is given by the following equations:

$$q_{\parallel t} = q_{\parallel e} + q_{\parallel i} \tag{5}$$

$$q_{\parallel e} = \gamma_e k T_{e0} \Gamma_0 \ (\gamma_e = 5.0) \tag{6}$$

$$q_{\parallel i} = \gamma_i k T_{i0} \Gamma_0 \left(\gamma_i = 2.5 + \frac{1}{2} M_t^2 \left[1.0 + \frac{T_{e0}}{T_{i0}} \right], \right.$$
$$\left. M_t = 1, T_{e0} = T_{i0} \right) \tag{7}$$

where $q_{\parallel e,i}$ is the electron/ion along-$\boldsymbol{B}$ power flow to the target, and $\gamma_{e,i}$ is the electron/ion heat transfer coefficient.

With the models stated above, this OSM solver can simultaneously start from both the inner and the outer target conditions to establish the 2D plasma conditions by analysing the parallel and cross-field balances sequentially and iteratively for the inner SOL and the outer SOL, defined in figure 2, separately.

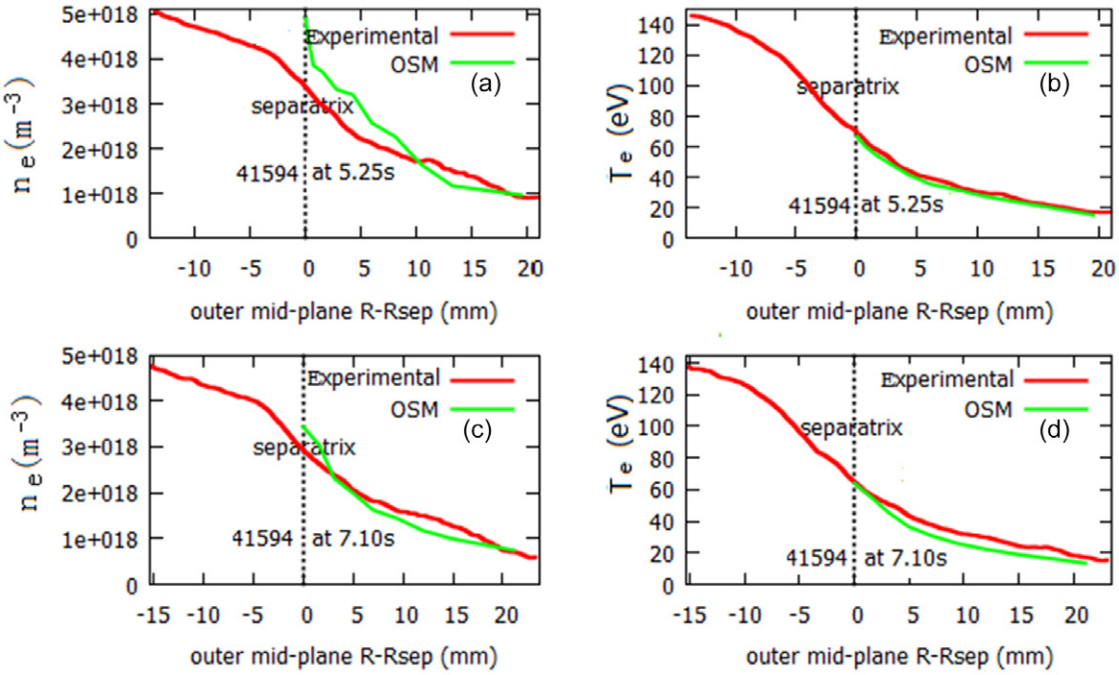

Figure 5. Outboard mid-plane values of n_e and T_e from the FRP compared with the values from the OSM versus distance from the separatrix for shot 41594 at 5.25 and 7.10 s.

4. OSM reconstruction of EAST SOL plasma conditions

4.1. Code–experiment comparison with FRP measurements at the outboard mid-plane

With the possession of data presented in section 3.1, one can carry out the OSM analysis using the models stated in section 3.2. As is mentioned above, the OSM solver chosen for simulations mentioned here is a half-ring from the target fluid equation solver (flow velocity zero at the mid-point of each flux tube) that can use sources/sinks specified and balanced for the full flux tube. In addition, due to the fact that sometimes quite different stories occur in the outer SOL and inner SOL, this solver provides a useful tool to analyse the inner and the outer SOLs separately [7, 12].

OSM-generated plasma conditions can be validated by comparisons between the calculated and the measured upstream plasma parameters. Figure 5 directly compares the FRP-measured values of the electron density and temperature at the outboard mid-plane with the OSM-generated outboard mid-plane values of n_e and T_e. The data are plotted as a function of distance from the separatrix. Because of the uncertainties in the separatrix location at the mid-plane, which is mentioned in section 2, the FRP-measured profiles shown in figure 4 are shifted so that the FRP-measured T_e values and the OSM-calculated T_e values match at the separatrix location. Typically, the shift is ~5–8 mm for profiles in figure 5. Figure 5 demonstrates favourable agreement between the values of the measured and the OSM-calculated outboard mid-plane n_e and T_e, especially for T_e.

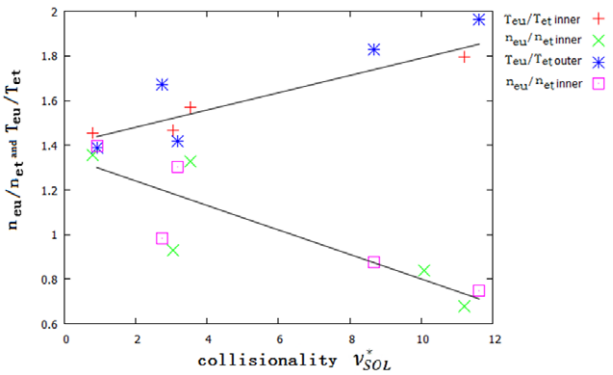

Figure 6. Ratio of SOL upstream to target density, and SOL upstream to target temperature, plotted as functions of collisionality ν^*_{SOL} in the SOL.

4.2. Other characteristics of SOL plasmas derived from the OSM

SOL collisionality, defined as the total connection length divided by the electron mean free path between collisions, is considered to be one critical factor determining the SOL plasma conditions. Checking the dependence of the OSM-calculated plasma conditions on the SOL collisionality can provide more details about the physics processes occurring in the SOL and help to validate the calculated results [8, 13]. According to [8], $\nu^*_{SOL} \approx 10^{-16} n_{eu} L_c / T_{eu}^2$, with T_{eu} in eV. The subscript 'u' denotes the upstream, defined as the mid-plane location here. The values of n_e and T_e at the outer mid-plane and at the inner mid-plane are used to calculate the collisionality for the outer SOL and the inner SOL separately. Figure 6 shows the ratio of OSM-generated upstream parameters to that of the Langmuir probe measurements for density and temperature (defining the target

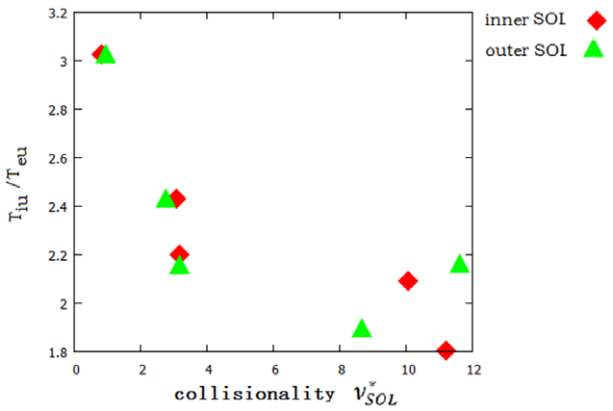

Figure 7. OSM-calculated ratio of upstream T_i to T_e versus SOL collisionality ν^*_{SOL}.

boundary condition in the OSM) of all the discharges shown in table 1. Values for the outer SOL and the inner SOL are obtained separately and are both shown in figure 6. This figure seems to give the same tendency as that found in [8], which finds that T_{eu}/T_{et} tends to increase with collisionality, while n_{eu}/n_{et} tends to decrease with collisionality, especially for the relatively high collisionality cases. There is no significant difference between the inner SOL and the outer SOL for this behaviour shown in figure 6.

Figure 7 shows the ratio of the OSM-calculated ion temperature to electron temperature at both the inboard and outboard mid-planes for all the discharges considered in the modelling. It clearly demonstrates that the calculated upstream ion temperature is around twice the electron temperature, which is consistent with the experimental finding in [21]. In addition, the ratio of the OSM-calculated ion temperature to electron temperature is found to decrease with the decrease in distance to the target along the flux tube, i.e. the increase in collisionality, due to the approach to electron–ion equipartition.

5. Extraction of cross-field transport coefficients from the OSM

One of the important applications of the OSM is the extraction of $D_\perp^{\rm SOL}$ and $\chi_\perp^{\rm SOL}$ by performing particle and power balance on the OSM-generated 2D plasma solutions [7, 8, 13, 20] using equations (8) and (9).

$$\Gamma_\perp A_\perp = S_{\rm i} - S_{\rm r} + \Gamma_{\parallel {\rm t}} A_{\rm t} \tag{8}$$

$$q_\perp A_\perp = P_{\rm vol} + q_{\parallel {\rm t}} A_{\rm t} \tag{9}$$

where $S_{\rm i}$ and $S_{\rm r}$ are the ionization and recombination sources, $\Gamma_{\parallel {\rm t}}$ and $q_{\parallel {\rm t}}$ are the parallel particle and power flux density to the targets, $A_\perp$ and $A_{\rm t}$ are the flux tube area along the separatrix and the target area, respectively, and $P_{\rm vol}$ is the total volumetric power loss/gain by the ions and electrons. The local values of the cross-field particle flux density, $\Gamma_\perp$, and heat flux density, $q_\perp$ are given by equations (10) and (11).

$$\Gamma_\perp = D_\perp^{\rm SOL} \frac{n}{\lambda_n} \tag{10}$$

$$q_\perp = \chi_\perp^{\rm SOL} \frac{nkT}{\lambda_T} + \frac{5}{2} D_\perp^{\rm SOL} \frac{nkT}{\lambda_n} \tag{11}$$

where λ_n and λ_T are the local radial scale lengths given by the OSM. The power balance can be performed for electrons and ions separately to extract $\chi_{\perp {\rm i}}^{\rm SOL}$ and $\chi_{\perp {\rm e}}^{\rm SOL}$. Also, one can perform the combined electron and ion power balance to get $\chi_\perp^{\rm SOL}$. The values of $\chi_\perp^{\rm SOL}$ and $D_\perp^{\rm SOL}$ can be extracted as a function of the radial location by carrying out the balance calculations for different portions of SOL.

Equations (8) and (9) illustrate that for reliable extraction of $D_\perp^{\rm SOL}$ and $\chi_\perp^{\rm SOL}$ one requires that the terms containing these variables are not very small compared with other terms, otherwise the errors and uncertainties will make the extracted values unreliable. For $D_\perp^{\rm SOL}$ extraction, unless the portion of ionization occurring inside the separatrix is not very small, the extracted values of $D_\perp^{\rm SOL}$ are unreliable. While this is not the case for $\chi_\perp^{\rm SOL}$ since the source of the power for the SOL is always the core, and the cross-field power terms must always at least be comparable to the other terms, which makes reliable $\chi_\perp^{\rm SOL}$ extraction possible. More details about the OSM method of $\chi_\perp^{\rm SOL}$, $D_\perp^{\rm SOL}$ extraction are given in [1, 7, 8].

The following part of this section will focus on the extraction of cross-field transport coefficients based on the OSM solution for EAST discharges introduced in section 4. Following the authors of [7, 25], before using the OSM method of $D_\perp^{\rm SOL}$ and $\chi_\perp^{\rm SOL}$ extraction for EAST discharges, a moderate recycling discharge with the SOL plasma conditions reconstructed by SOLPS is chosen to carry out the code–code comparison between OSM–EIRENE and SOLPS. Details are shown as follows.

5.1. Validation of the OSM method of $\chi_\perp^{\rm SOL}$ and $D_\perp^{\rm SOL}$ extraction for the EAST case

There are two reasons why the OSM approach can be an effective and widely used approach to study the cross-field transport property of SOL plasmas. One reason is that the cross-field transport is implicitly included in the experimental data used as boundary conditions for the OSM calculation. The other reason is that OSM can reliably establish the 2D profiles in an effective way. These two points will be demonstrated here by taking target n and T profiles generated by SOLPS and comparing the values of the cross-field transport coefficient with those used as input for the SOLPS calculation.

For reliable extraction of particle diffusivity, $D_\perp^{\rm SOL}$, and for full comparison between SOLPS and OSM, a moderate divertor recycling EAST case with heating power $P_{\rm in} = 0.35$ MW, line-averaged density $\bar{n}_{\rm e} = 0.98 \times 10^{19}$ m^{-3}, ~15% of ionization occurring inside the separatrix is chosen for use. The assumptions used for the SOLPS calculation are as follows: $\chi_{\perp {\rm i}}^{\rm SOL} = \chi_{\perp {\rm e}}^{\rm SOL} = 1.0\,{\rm m^2\,s^{-1}}$, $D_\perp^{\rm SOL} = 0.5\,{\rm m^2\,s^{-1}}$. Figures 8 and 9 provide a direct comparison between the OSM-calculated along-$\boldsymbol{B}$ profiles of plasma parameters, $n_{\rm e}(s)$, $T_{\rm e}(s)$, $T_{\rm i}(s)$ and $V_{\rm b}(s)$ for the second (3 mm from the separatrix at the outboard mid-plane) and the seventh (12 mm from the separatrix at the outboard mid-plane) SOL grid ring, respectively, giving a favourable consistency for the four quantities shown here. Here s is the distance measured along-$\boldsymbol{B}$ from target to target. For all the plots shown here, the inner target is on the left and the outer target is on the right-hand side.

After the OSM calculation, one has all the volumetric sinks/sources, the target power and particle fluxes, as well as all

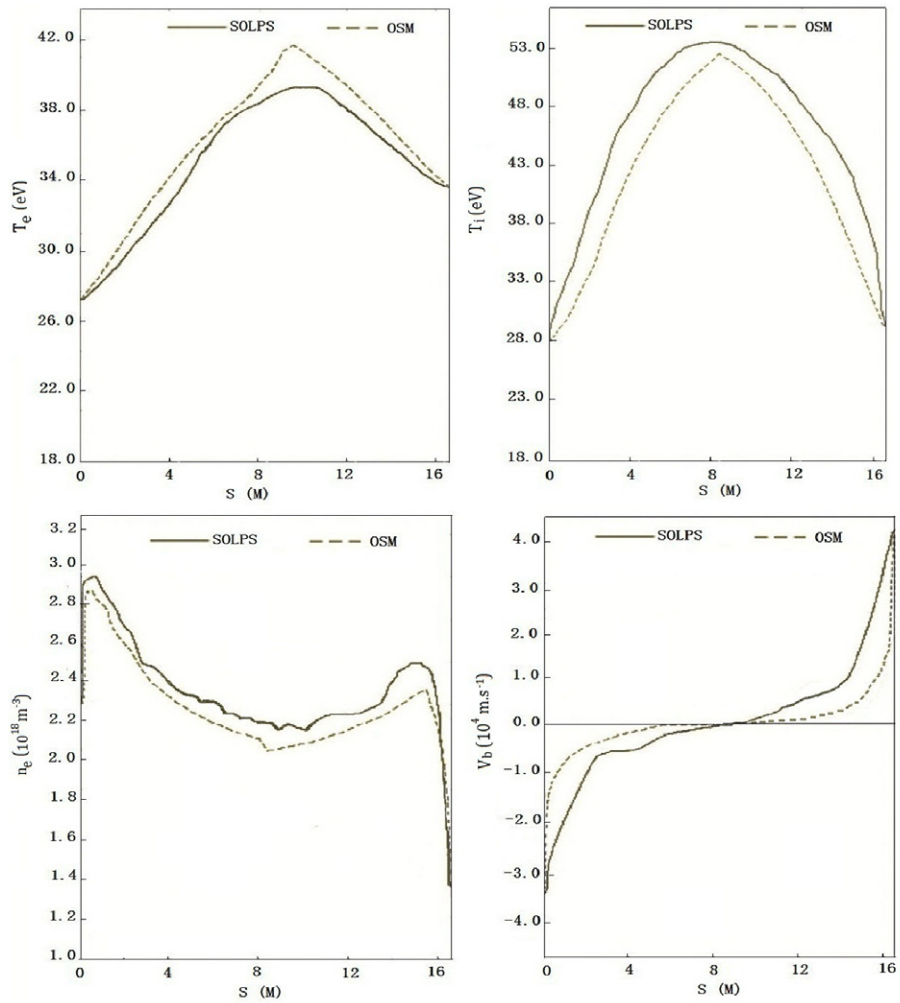

Figure 8. 'Moderate recycling' EAST case; second SOL grid ring (3 mm from the separatrix at the outboard mid-plane). n_e, T_e, T_i, V_b as a function of s, measured along B from the inner target to the outer target; solid line: SOLPS; dashed line: OSM.

the radial gradients, so that one can perform a straightforward particle/power balance calculation to extract $D_\perp^{SOL}$ and $\chi_\perp^{SOL}$. By carrying out a balance calculation for different parts of the SOL, one can extract $D_\perp^{SOL}$ and $\chi_\perp^{SOL}$ as a function of the radial distance. $D_\perp^{SOL}$ and $\chi_\perp^{SOL}$ can be extracted essentially from the experimental data, which is the focus of the following part of this section. Here, we use the extraction procedure as a test of the OSM method of $D_\perp^{SOL}$ and $\chi_\perp^{SOL}$ extraction.

Figure 10 shows the values of $D_\perp^{SOL}$, $\chi_{\perp i}^{SOL}$, $\chi_{\perp e}^{SOL}$ and $\chi_\perp^{SOL}$ as a function of r (measured at the outboard mid-plane) extracted from the OSM solution and compared with the inputs used in the SOLPS calculation. This comparison gives agreement within a factor of less than 2. $\chi_\perp^{SOL}$ is a quantity extracted using the combined electron and ion power balance. The volume power terms were included in the OSM method of extraction. Since this case is chosen deliberately with sufficient neutrals ionized (typically, ~15% shown by the EIRENE calculation) inside the separatrix to provide a reasonably strong cross-field particle flow, the $D_\perp^{SOL}$ value extracted in this case is expected to be reliable. The cross-field convection is included in the power balance to extract $\chi_\perp^{SOL}$ by performing the $D_\perp^{SOL}$ extraction first.

5.2. OSM extraction of heat diffusivity $\chi_\perp^{SOL}$

As mentioned above, reliable extraction of a cross-field particle transport coefficient needs that the portion of ionization occurring in the region inside the separatrix is not very small. This requirement cannot be well satisfied for all the discharges listed in table 1. However, $\chi_\perp^{SOL}$ can be extracted from equations (8) and (9) by assuming some ratio of $D_\perp^{SOL}/\chi_\perp^{SOL}$, typically 0.4 in other tokamaks [8, 13], and $\chi_\perp^{SOL}$ is demonstrated to be fairly insensitive to this ratio in the range 0.2–0.6 [13].

Figure 11 shows the resulting $\chi_\perp^{SOL}(r)$ profiles at both the inner and outer mid-planes for discharges with main characteristics shown in table 1. From figure 11, most radial profiles show an increase in $\chi_\perp^{SOL}(r)$ with radius. Some profiles reach maxima and show a subsequent fall far out in the SOL where T_e scale lengths and J_{sat} are difficult to be measured; hence this feature may not be practical or could be a transition to the less collisional regime. The increasing tendency of the $\chi_\perp^{SOL}(r)$ profile corresponds to the fact that the $T(r)$ profile tends to flatten with increasing radius r, which also highlights the fact that $\chi_\perp^{SOL}$ has a collisionality dependence, n/T^2, i.e. that the anomalous transport assumption is consistent with

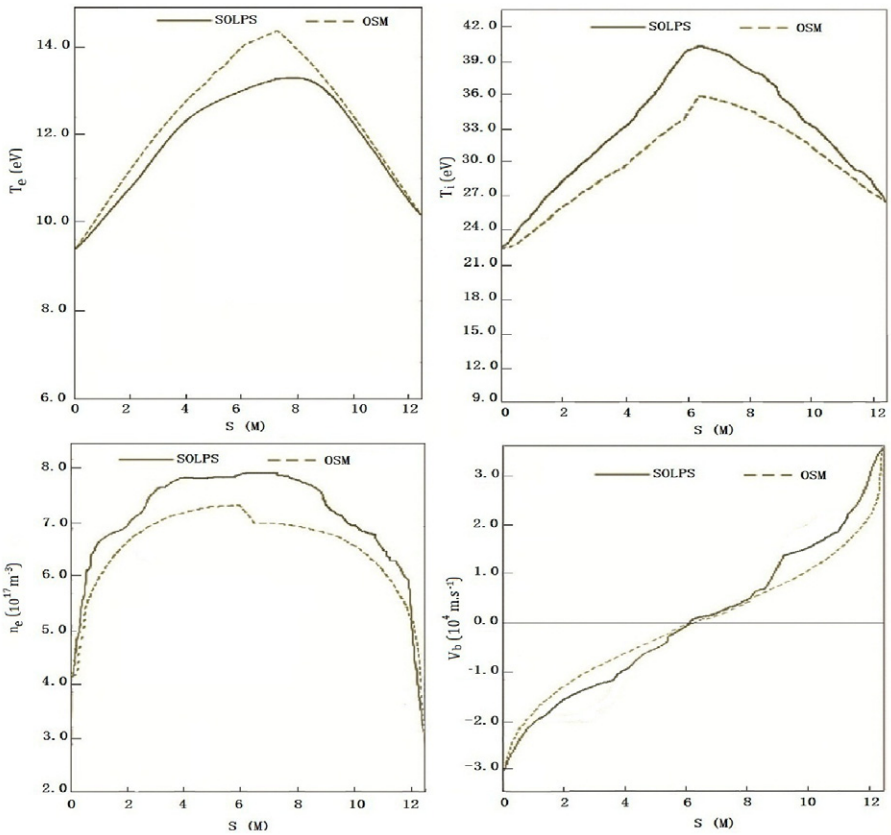

Figure 9. As for figure 8 but the seventh grid ring (12 mm from the separatrix at the outboard mid-plane).

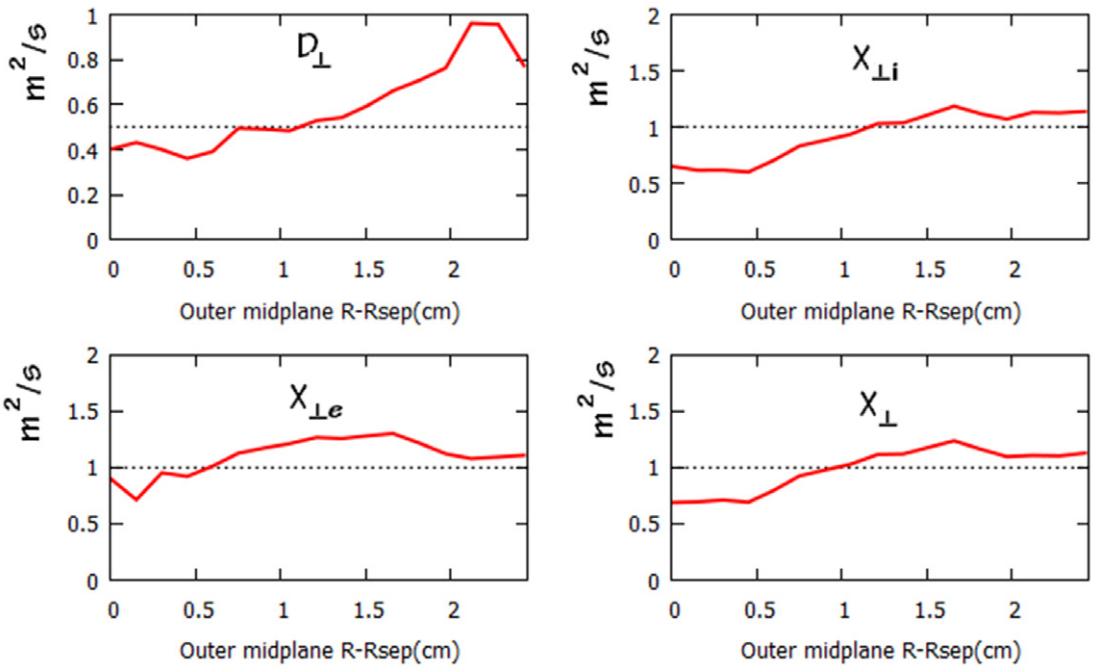

Figure 10. Extracted $D_\perp^{\mathrm{SOL}}$, $\chi_{\perp\mathrm{i}}^{\mathrm{SOL}}$, $\chi_{\perp\mathrm{e}}^{\mathrm{SOL}}$ and $\chi_\perp^{\mathrm{SOL}}$ for a moderate EAST discharge. Transport coefficients from the OSM solutions as a function of ring location at the outboard mid-plane are plotted with solid lines. SOLPS inputs plotted with dashed lines.

the results from the drift-wave instability driven turbulence. As can be seen from figure 11, most of the outboard values of $\chi_\perp^{\mathrm{SOL}}(r)$ are greater than those at the inboard mid-plane, which is consistent with the Bohm-like scaling prediction, $\chi_\perp^{\mathrm{SOL}} \propto B^{-1}$. Note that the values of $\chi_\perp^{\mathrm{SOL}}(r)$ for the inner SOL and that for the outer SOL are plotted with different scales in figure 11. However, to get the detailed scaling expression for the relation between the thermal heat diffusivity

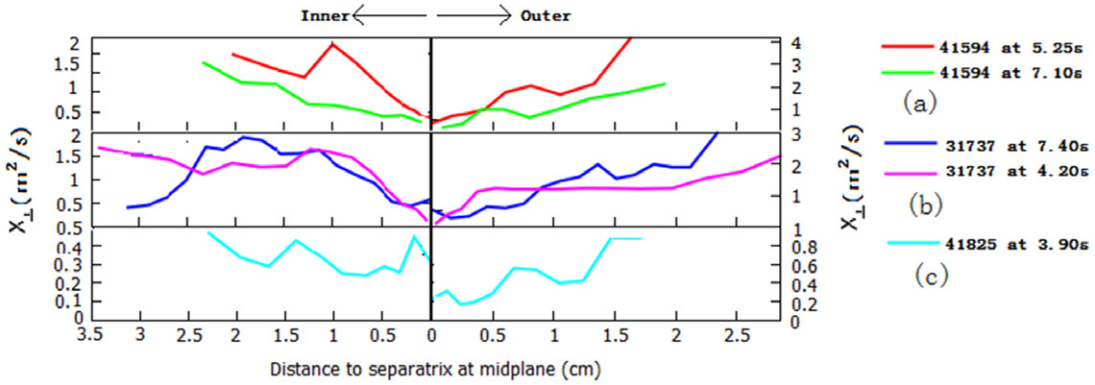

Figure 11. OSM-extracted $\chi_{\perp}^{\mathrm{SOL}}(r)$ profiles at both the inner and outer mid-planes for EAST discharges with main characteristics listed in table 1.

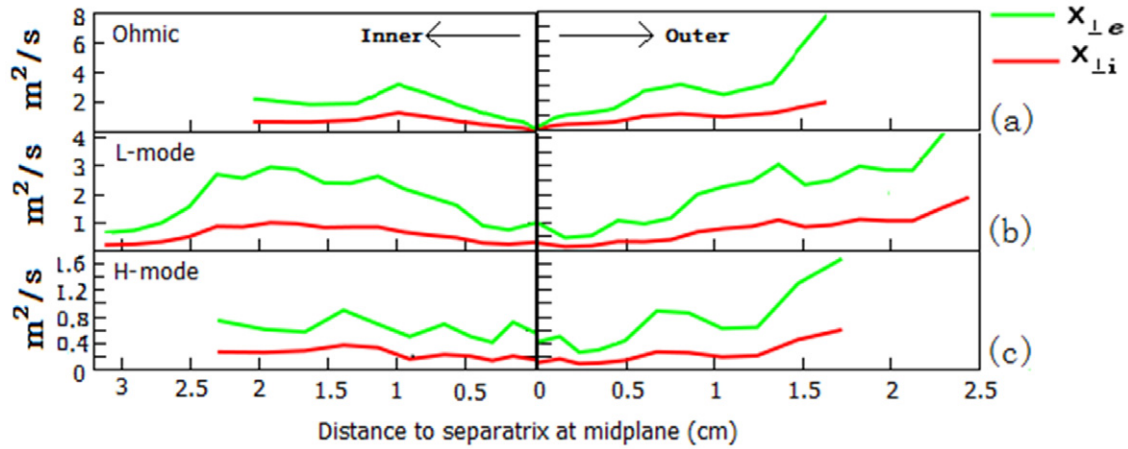

Figure 12. OSM-extracted $\chi_{\perp\mathrm{i}}^{\mathrm{SOL}}(r)$ and $\chi_{\perp\mathrm{e}}^{\mathrm{SOL}}(r)$ profiles at both the inner and outer mid-planes for discharges with a LSN divertor configuration selected from table 1.

$\chi_{\perp}^{\mathrm{SOL}}$ and the SOL plasma parameters, future work will be performed to consider much more discharges with a wide range of parameters. This paper, here, just gives some qualitative description of the heat transport property in EAST.

Note that the quantity in figure 11 is $\chi_{\perp}^{\mathrm{SOL}}$ extracted using the combined electron and ion power balance. The electron thermal heat diffusivity, $\chi_{\perp\mathrm{e}}^{\mathrm{SOL}}$, is found to be higher by a factor of 2–3 than the ion thermal heat diffusivity $\chi_{\perp\mathrm{i}}^{\mathrm{SOL}}$, which is also found by Erents *et al* in [20]. Figure 12 gives a direct description of $\chi_{\perp\mathrm{e}}^{\mathrm{SOL}}(r)$ and $\chi_{\perp\mathrm{i}}^{\mathrm{SOL}}(r)$ profiles at both the outer and inner mid-planes for three discharges with a LSN divertor configuration shown in table 1.

6. Summary and conclusions

An OSM solver coupled with DIVIMP has been used in combination with the Monte Carlo neutral transport code EIRENE to calculate two-dimensional distributions of the SOL plasma conditions (T_{e}, T_{i}, n_{e}, V_{b}) in EAST. Based on the boundary conditions measured by Langmuir probes built into the divertor targets, ohmic, L- and H-mode discharges with single-null divertor configurations have been analysed and the mid-plane values of the electron density and temperature obtained by the OSM have been compared with the experimental measurements from a fast reciprocating probe setup at the outboard mid-plane. The OSM can reconstruct the EAST SOL upstream plasma conditions with favourable consistency, especially taking into consideration the uncertainties in the interpretation of probe data. In addition, some other results about the EAST SOL plasmas derived from the OSM have also been discussed, reflecting that the upstream plasma conditions are governed by the SOL collisionality to a large degree.

By taking target profiles generated by SOLPS, the reliability of the OSM method of cross-field transport coefficients, $D_{\perp}^{\mathrm{SOL}}$ and $\chi_{\perp}^{\mathrm{SOL}}$, extraction has been assessed, which enhances the confidence to use the OSM-based method to carry out a preliminary study on the heat transport property in EAST SOL. $\chi_{\perp}^{\mathrm{SOL}}(r)$ profiles at both the inner and outer mid-planes for discharges with main characteristics shown in table 1 have been extracted, finding that most of the values of $\chi_{\perp}^{\mathrm{SOL}}(r)$ at the outer mid-plane are larger than that at the inner mid-plane, clearly demonstrating a ballooning-like transport regime $\sim 1/B$. Moreover, the increase in $\chi_{\perp}^{\mathrm{SOL}}$ with decreasing temperature or increasing density shows at least some consistency with a collisionality dependence as suggested by drift-wave driven turbulence. By performing the electron and ion power balance separately, the OSM-extracted $\chi_{\perp\mathrm{e}}^{\mathrm{SOL}}$ is found to be larger than $\chi_{\perp\mathrm{i}}^{\mathrm{SOL}}$ by a factor of 2–3. However, to find a detailed relation between the SOL heat

diffusivity $\chi_{\perp}^{\mathrm{SOL}}$ and the SOL parameters, future work should be performed, considering many more discharges with a wide range of parameters.

Having validated the OSM–EIRENE–DIVIMP code with comparisons against experimental data presented in this paper, we are now in a position to produce a more extensive $\chi_{\perp}^{\mathrm{SOL}}$ database for EAST with target data measured by built-in Langmuir probes for most discharges. These results as well as DIVIMP impurity related study on EAST will be reported on later.

Acknowledgments

This work was sponsored by the National Natural Sciences Foundation of China (Nos. 11261140328 and 10975158) and the National Magnetic Confinement Program (2013GB107003). The authors are very grateful to the EAST team for all the experimental measurements and the discussion about the experimental details.

References

[1] Stangeby P.C. 2000 *The Plasma Boundary of Magnetic Fusion Devices* (Bristol: Institute of Physics Publishing)
[2] Stangeby P.C., Canik J.M. and Whyte D.G. 2010 *Nucl. Fusion* **50** 125003
[3] Schneider R. *et al* 2006 *Contrib. Plasma Phys.* **46** 3
[4] Stangeby P.C. 1990 *Nucl. Fusion* **30** 1225
[5] Reiter D. *et al* 1984 *Jeulich Report* JUEL-1947 Maascrict, 14–18 June 1999
[6] Reiter D. *et al* 2005 *Fusion Sci. Technol.* **47** 172 www.ans.org/pubs/journals/fst/a_698
[7] Monk R.D. *et al* 1995 *J. Nucl. Mater.* **220–222** 612
[8] Erents S.K. and Stangeby P.C. 1998 *Nucl. Fusion* **38** 1637
[9] Erents S.K. *et al* 2000 *Nucl. Fusion* **40** 295
[10] Erents S.K. *et al* 2000 *Nucl. Fusion* **40** 309
[11] Kirk A. *et al* 2003 *Plasma Phys. Control. Fusion* **45** 1445
[12] Stangeby P.C. 2001 *J. Nucl. Mater.* **290–293** 733
[13] Kirk A. *et al* 2004 *Plasma Phys. Control. Fusion* **46** 1591
[14] Wan B.N. *et al* 2009 *Nucl. Fusion* **49** 104011
[15] Wang L. *et al* 2012 *Nucl. Fusion* **52** 063024
[16] Zhang L. *et al* 2011 *Plasma Sci. Technol.* **13** 431
[17] Liu S.C. *et al* 2012 *Phys. Plasmas* **19** 042505
[18] Elder J.D. *et al* 2006 *J. Nucl. Mater.* **337–339** 79
[19] Elder J.D. *et al* 2007 *J. Nucl. Mater.* **363–365** 147
[20] Erents S.K. *et al* 1997 *J. Nucl. Mater.* **241–243** 433
[21] Guo H.Y. *et al* 1996 *Contrib. Plasma Phys.* **36** 81
[22] Stangeby P.C. *et al* 1990 *Nucl. Fusion* **30** 1225
[23] Stangeby P.C. *et al* 1988 *Nucl. Fusion* **28** 1945
[24] Loarte A. and Harbour P.J. 1992 *Nucl. Fusion* **32** 681
[25] Stangeby P.C. *et al* 1997 *J. Nucl. Mater.* **241–243** 358
[26] Shimizu K. *et al* 1992 *J. Nucl. Mater.* **196–198** 258
[27] Eich T. *et al* 2011 *Phys. Rev. Lett.* **107** 215001